Numerical simulations for the bearing capacity of strip footings

Dalia S. Youssef Abdel Massih[1] and Abdul-Hamid Soubra[2], M. ASCE.

[1] PhD Student, University of Nantes & Lebanese University, BP 11-5147, Beirut, Lebanon. E-mail: Dalia.Youssef@univ-nantes.fr

[2] Professor, University of Nantes, GeM, UMR CNRS 6183, Bd. de l'université, BP 152, 44603 Saint-Nazaire cedex, France. E-mail: Abed.Soubra@univ-nantes.fr

Abstract

The aim of this paper is the computation of the failure loads of a rough rigid strip footing subjected to a vertical, inclined or eccentric loading using the finite difference code $FLAC^{3D}$. For the case of vertical load, controlled downward vertical velocities are applied to the footing nodes until a steady state of plastic flow is obtained in the soil. For the construction of the (H,V) failure envelope of an inclined load, a uniform normal stress distribution is first applied to the base of the footing and the system is solved until it reaches an equilibrium state. Then, controlled horizontal velocities are applied to the nodes of the footing bottom until a steady state of plastic flow is obtained in the soil. For the (M,V) failure envelope of an eccentric load, a vertical downward velocity is applied at various eccentricities. For each eccentricity, damping of the system is performed until a steady state of plastic flow is developed in the soil. Results of failure loads are presented and compared with those of other authors.

Introduction

The ultimate bearing capacity of a strip footing subjected to a central vertical load has long been a topic for research. However, when the footing is subjected to an inclined or an eccentric load, the scientific research concerning this problem has essentially occurred during the last few decades. Traditionally, geotechnical engineers make use of empirical reduction coefficients provided by the different codes. The numerical simulations concerning this issue are less extensive than for the case of a vertically loaded footing. In this paper, numerical simulations of the failure loads of a rough rigid strip footing subjected to a vertical, inclined or eccentric loading are performed using the Lagrangian explicit finite difference code $FLAC^{3D}$.

Numerical Simulations

This section focuses on the numerical modeling of the failure loads of a rough rigid strip footing, of breadth *B=2 m*, resting on a $c-\varphi$ soil.

FLAC^{3D} (Fast Lagrangian Analysis of Continua) is a commercially available three-dimensional finite difference code in which an explicit Lagrangian calculation scheme and a mixed discretization zoning technique are used. This kind of discretization enables one to obtain a constant limit load and not a steadily rising load-displacement curve as it the case in traditional finite elements and finite difference methods. This is because the mixed discretization scheme reduces the number of constraints on plastic flow. It should be mentioned that $FLAC^{3D}$ includes an internal programming option (*FISH*) which enables the user to add his own subroutines. The soil domain is divided by the user into a *3D* finite difference mesh of polyhedral zones. Constant strain-rate elements of tetrahedral shape whose vertices are the nodes of the mesh are used. This enables the velocity field to be linear inside the tetrahedrons. Each element behaves according to a prescribed linear or nonlinear stress/strain law in response to applied forces or boundary restraints. Several constitutive models are available. It should be noted that $FLAC^{3D}$ code is particularly suited for problems involving limit loads and steady plastic flow. In this code, although a static (*i.e.* non-dynamic) mechanical analysis is required, the equations of motion are used. The solution to a static problem is obtained through the damping of a dynamic process by including damping terms that gradually remove the kinetic energy from the system. *Local nonviscous damping* is used. The damping force is equal to 80 % of the out-of-balance force defined below. For further details, one can refer to $FLAC^{3D}$ manual.

The theoretical background of the $FLAC^{3D}$ code can be summarized as follows: The equations of motion of an equivalent static problem involving inertial terms were written in a discrete form at the different nodes of the discretized medium. This enables one to transform the equations of motion of the continuum into a set of Newton's law at the nodes of the mesh. The later equations constitute a system of differential equations which are solved using the Lagrangian explicit finite difference scheme in time. The new idealized medium can be viewed as an assembly of point masses located at the nodes of the mesh and connected by linear springs since the system of ordinary differential equations obtained is similar to that describing the motion of a mass-spring system. The analogy with the idealized medium is immediate if one interprets the statically equivalent nodal force of all contributing tetrahedra and nodal applied loads (called hereafter out-of-balance force) as the resultant of spring reactions and external applied forces in the mass-spring system. The out-of-balance forces of all nodes are equal to zero when the medium has reached equilibrium. In the present numerical model, the inertial terms are used as means to reach, in a numerically stable manner, the steady state of static equilibrium or plastic flow. This is performed by replacing the mass involved in the inertial term by a fictitious nodal mass whose value ensures numerical stability of the system on its route to steady state. The calculation scheme invokes equations of motion in their discretized forms (*i.e.* Newton's law at the different nodes) to derive new velocities and displacements from stresses and forces. Then, strain rates are derived from velocities, and new stresses from strain rates. The stresses and deformations are calculated at several small timesteps (called hereafter cycles) until a steady state of static equilibrium or plastic flow is achieved. The convergence to this state may be controlled by a maximal prescribed value of the unbalanced force for all elements of the model. In *FLAC*^{3D}, the application of velocities or stresses on a boundary creates unbalanced forces in the system. Damping is introduced in order to remove these forces or to reduce them to small values compared to the initial ones.

Vertical load

Because of symmetry, only half of the entire soil domain of width *20B* and depth *5B* is considered. The horizontal and right vertical boundaries are far enough from the footing and they do not disturb the soil mass in motion (*i.e.* velocity field) for all the soil configurations studied in this paper. A non uniform mesh composed of 904 zones is used. For the half mesh on the right hand side, the region under the footing was divided horizontally into *15* zones, which size gradually decreases from the center to the edge of the footing where very high stress gradients are developed. Beyond the edge of the footing, the domain was divided into *30* zones which size increases gradually from the foundation edge to the right vertical boundary. Vertically, the domain was divided into *20* zones which size decreases gradually from the bottom of the domain to the ground surface. Since this is a *2D* case, all displacements in the direction parallel to the footing are fixed. For the displacement boundary conditions, the bottom boundary was assumed to be fixed and the vertical boundaries were constrained in motion in the horizontal direction. A conventional elastic-perfectly plastic model based on the Mohr-Coulomb failure criterion is used to represent the soil. The soil elastic properties used are the shear modulus $G = 100\,MPa$ and the bulk modulus $K = 133\,MPa$. The values of the soil shear strength parameters used in the analysis will be given in the next sections. A strip footing of width equal to $2\,m$ and depth $0.5\,m$ is simulated by a weightless elastic material. It is divided horizontally into eight zones. The footing elastic properties used are the Young's modulus $E = 25\ GPa$ and the Poisson's ratio $\nu = 0.4$. Compared to the soil elastic properties, these values are well in excess of those of the soil and ensure a rigid behavior of the footing. Notice that the soil and footing elastic properties have a negligible effect on the failure load. The footing is connected to the soil via interface elements that follow Coulomb law. The interface is assumed to have a friction angle equal to the soil angle of internal friction, dilation equal to that of the soil and cohesion equal to the soil cohesion in order to simulate a perfectly rough soil-footing interface. Normal stiffness $K_n = 10^9\ Pa/m$ and shear stiffness $K_s = 10^9\ Pa/m$ are assigned to this interface. These parameters do not have a major influence on the failure load.

For the computation of the bearing capacity of a rigid rough strip footing subjected to a central vertical load using *FLAC*^{3D}, two methods are used. They are presented in the next sections. In all the simulation methods described below, the following procedure is adopted (when applicable) before any simulation of the foundation load: Geostatic stresses are first applied to the soil, then several cycles are run in order to arrive to a steady state of static equilibrium and finally, the obtained displacements are set to zero in order to obtain the footing displacement due to only the footing load.

Method 1: In this method, a controlled downward vertical velocity (*i.e.* displacement per timestep) is applied to the nodes of the footing. Damping of the system is performed by running several cycles until a steady state of plastic flow is developed in the soil underneath the footing. This state is achieved when both conditions (i) a constant footing load and (ii) small values of unbalanced forces, were satisfied as the number of cycles increases. The number of cycles required to reach this state depends on the value of the applied velocity. At each cycle, the vertical footing load is obtained by using a FISH function that calculates the integral of the normal stress components for all elements in contact with the footing. The value of the vertical footing load at the plastic steady state is the ultimate footing load. The ultimate bearing capacity is then obtained by dividing this load by the footing area. Several control parameters, such as the intensity of the vertical velocity and the mesh size, may greatly affect the value of the ultimate footing load. An optimal vertical velocity must be chosen in order to reach a value of the bearing capacity close to the smallest most critical one (corresponding to very small velocity) with a reasonable computation time. A velocity of 2.5×10^{-6} m/timestep downward was suggested by Yin et al. (2001) as a result of a number of verification runs. This value was checked and was found to be an optimal one if cohesion is present in the soil. However, when dealing with sand, a smaller velocity of 10^{-7} m/timestep was found necessary to reach the optimal results. An ultimate load of *2393.1* kN/m was obtained at the plastic steady state (for which a continuous increase in the displacement is obtained for a constant footing load) when $\varphi=\psi=30°$ and $c=20\ kPa$ where ψ is the soil dilation angle (*cf.* Figure 1). The effect of the mesh size on the solution was also checked. It was found that a more refined mesh under the footing does not improve the value of the footing load and may cause numerical instability. A more refined mesh beyond the edge of the footing improves the result (*i.e.* reduces the ultimate load) by only *0.27 %* with an increase in the calculation time by *36%*. Thus, the mesh presented above will be used in all subsequent calculations.

Method 2: In this method, the same soil shear strength parameters, the same soil and footing elastic properties and the same interface characteristics used in Method 1 are considered in the present section and in the next two sections. Incremental (*i.e.* gradually increasing) vertical nodal stresses are applied to the nodes situated at the base of the footing. For each stress increment, damping is performed until a steady state is obtained. For the different stress levels, the vertical displacement at the center of the footing bottom is computed and the footing load is obtained using the same FISH function of *Method 1*. The value of the footing load corresponding to a continuous increase of the displacement represents the ultimate footing load. Its value was found equal to *2394.44* kN/m which is close to the value calculated by the previous method (*cf.* Figure 1). However, in the present method, the number of cycles required to achieve a steady state of plastic flow depends on the stress increment value. Also, an increase in the number of cycles is necessary in the neighborhood of the failure load thus requiring very high computation time. Consequently, this method is found to be less efficient than the first one. Thus, Method 1 which is a displacement-controlled procedure will be used for the simulation of the bearing capacity of a vertically loaded footing. Two other displacement-controlled procedures are used for the simulation of an ultimate inclined or eccentric load. They are presented in the next two sections.

Inclined load

Because of the absence of loading symmetry, the entire soil domain of dimensions $(20B\,x\,5B)$ will be considered in this section and in the next section. The numerical simulation procedure used for the computation of the (H,V) failure envelope (where H and V are the horizontal and vertical ultimate footing loads respectively) can be summarized as follows: Firstly, a central vertical load (smaller than the ultimate vertical one) is applied to the footing *via* uniform nodal stresses acting at the nodes situated at the base of the footing. Damping of the system is introduced by running several cycles until a steady state of static equilibrium is developed in the soil. Secondly, a controlled horizontal velocity is applied to the nodes situated at the footing bottom. Again, damping of the system is performed by running several cycles until a steady state of plastic flow is developed in the soil underneath the footing. At each cycle, the horizontal footing load is obtained by using a FISH function that calculates the integral of the shear stress components for all elements in contact with the footing. The value of the horizontal load at the plastic steady state is the ultimate horizontal load that led to soil failure. The corresponding horizontal footing stress is obtained by dividing this load by the footing area. The ultimate bearing capacity is obtained by dividing the vertical applied load by the footing area.

Eccentric load

For an eccentric load, one applies a given downward vertical velocity at various eccentricities at the base of the footing. For each eccentricity (e), damping of the system is performed by running several cycles until a steady state of plastic flow is developed in the soil underneath the footing. At each cycle, the (M, V) failure point (where M and V are respectively the moment and vertical load at the centre of the footing) is determined by integration of the normal stresses along the interface elements in contact with the footing using a FISH function. The ultimate bearing capacity is computed by dividing the obtained vertical load by the area of the footing.

Numerical results

For each type of soil, several runs are done in the aim to get the optimal velocity. As most of the methods used in bearing capacity assume (often implicitly) the associative flow rule, the computations are performed here for a dilation angle equal to the angle of internal friction in order to enable a fair comparison with other authors' results.

Vertical load

The results of the numerical simulations for the case of a vertically loaded footing are presented in the form of bearing capacity factors N_γ and N_c. Tables (1) and (2) present a comparison of the factors obtained from *FLAC*^{3D} and those given by other authors. The N_γ values obtained from *FLAC*^{3D} are close to the ones given by Yin et al. (2001), Soubra (1999), Vesic (1973) and Eurocode 7. However, Frydman and Burd (1997) solutions were found to be very high compared to all others. Also, one may notice that the present numerical N_γ values are higher than the ones given by Hjiaj et al. (2004) and Meyerhof (1951). For the N_c values, it was found that the present $FLAC^{3D}$ solutions are nearly identical to those of Yin et al. (2001). However, these solutions are greater than the closed-form solutions given by Prandtl (1920). This finding is similar to that of Zhu and Michalowski (2005) and Manoharan and Dasgupta (1995) who used elasto-plastic schemes for the computation of the bearing capacity factors. This may be explained as follows: The soil mass in motion (*cf.* velocity field) predicted by an elasto-plastic solution is more extended than that confined within Prandtl mechanism for the N_c factor (*cf.* Figure 2a). However, for the N_γ factor, the soil mass in motion is nearly similar in both elasto-plastic (Finite element and finite difference) and rigid-plastic (limit analysis) approaches (*cf.* Figure 2b). For the N_γ case, the velocity field is not very clear because of the high soil velocities at the footing edges compared to other points in the soil mass.

Table 1: Comparison of N_γ values

φ	FLAC ^{3D}	Yin et al.	Soubra	Vesic	Euro-code 7	Frydman et al.	Hjiaj et al.	Mey-erhof
30	19.23	20	21.5	22.40	20.1	21.7	14.9	15.7
35	46.1	46	49	48.03	45.2	54.2	34.8	37.1
40	119.7	120	119.8	109.3	106.0	147	85.8	93.6

Table 2: Comparison of N_c values

φ	FLAC^{3D}	Yin et al.	Manoharan et al.	Zhu et al. (Abaqus)	Prandtl
30	34	34.5	33	31.5	30.13
35	53.6	53	49	50	46.12
40	88.0	86	-	79	75.25

Inclined load

The results are presented here in the form of failure envelopes called also interaction diagrams. Two cases are considered: (i) a purely cohesive undrained clay with $c_u = 50\, kPa$ and, (ii) a cohesionless ponderable soil with $\varphi = 30°$. As mentioned before, only in the case of sand, a very small velocity of 10^{-7} m/timestep was necessary. In all other cases where the cohesion was present, a velocity of $2.5x10^{-6}$ m/timestep was found sufficient to give optimal results. Figures (3a, b) show the failure envelopes obtained from the numerical $FLAC^{3D}$ simulations and those of other authors. $FLAC^{3D}$ overestimates the Prandtl solution for an undrained clay due to the fact that the elasto-plastic analysis led to a more extended soil mass in motion than the classical Prandtl mechanism (figure not presented in this paper). For the sand, one can notice that $FLAC^{3D}$ numerical simulations are situated in between authors' solutions. Very close results to the Eurocode 7 were found. $FLAC^{3D}$ results were found to be smaller than Vesic's solutions. In contrast, the present solutions overestimate the results given by Meyerhof. Compared to the limit analysis solution given by Soubra et al. (2003a), *FLAC*^{3D} underestimates the solution for high values of the vertical applied load V and gives slightly higher results for smaller V values. Normal (σ) and shear (τ) stress distributions corresponding to different points of the failure envelope are presented in figures (5a, b) for the clay and the sand. For the clay, except at the footing edges which are singular points, a quasi-uniform normal stress distribution was observed. For the shear stress distribution, both positive and negative shear stresses are observed for large vertical loads (*cf.* Figure 5a). However, for small vertical loads corresponding to large horizontal loads, the shear stresses become all negative in order to counter weight the horizontal external load. At the limit, when the vertical load becomes smaller than or equal to 300 kN/m (*cf.* Figure 3a), the shear stresses tend to a constant value equal to $c_u = 50\,kPa$. This case corresponds to a sliding along the soil-footing interface. For the sand, a quasi-uniform normal stress distribution was observed near the footing center. It tends to zero at the edges of the footing. Concerning the shear stress distribution, as before both positive and negative shear stresses are observed for large vertical loads (*cf.* Figure 5a, b). However, for small vertical loads, the shear stresses become essentially negative. As for the normal stress distribution, the shear stress tends to zero at the footing edges.

Eccentric load

As for the vertical and inclined loading, only in the case of sand, a 10^{-7} m/timestep velocity was necessary. In all other cases where cohesion was present, a velocity of 10^{-6} m/timestep was found sufficient to give optimal results. It is to be mentioned that no tension at the soil-footing interface was considered. Figures (4a, b) show the failure envelopes obtained from *FLAC*^{3D} simulations and those of other authors for both the clay and the sand. The same conclusions stated for the inclined load remain valid here except for the limit analysis solutions by Soubra et al. (2003b) in the case of sand. For all eccentricities, it was found that *FLAC*^{3D} solutions are smaller than Soubra's ones. The distributions of normal stresses at the soil-footing interface have shown a gradually increasing separation distance at the left edge of the footing with the eccentricity increase for both the clay and the sand. The separation occurs once $e/B \geq 0.1$ where normal and shear stresses become equal to zero (*cf.* Figure 6a, b). The difference between the two normal stress distributions is that the normal stress decreases to zero at the right edge of the footing in the case of sand. However, a constant non-zero value was obtained for the clay. For the shear stress, a non-symmetrical distribution was observed with a gradually increasing separation distance with the eccentricity increase but the total horizontal footing load was found close to zero which is in conformity with the assumption of a vertical (non-inclined) load.

Conclusion

Numerical simulations of the failure loads of a strip footing subjected to a vertical, inclined or eccentric load were performed. It was shown that displacement-controlled and load-controlled approaches give close results. The displacement-controlled approach was used in all the computations since it requires less computation time. It was shown that *FLAC^{3D}* results are close to those given by the limit analysis for the ponderable soil and are greater than those of the limit analysis for a weightless soil. This was explained by the same volume of the soil mass in motion for only the ponderable soil. The weightless soil exhibits a difference in the soil mass in motion predicted by both approaches. It should be noted that *FLAC^{3D}* results are in good agreement with Eurocode 7 solutions. The distribution of the normal stress at the soil-footing interface has shown that in the case of an inclined load, the normal stress is quasi-uniform for clay and decreases to zero at the edges for the sand. However, for the eccentric load, the distribution shows a gradually increasing separation distance at the left edge of the footing with the eccentricity increase for both the clay and the sand. The difference between the two is that the normal stress decreases to zero at the right edge of the footing in the case of sand. Concerning the shear stress distribution, both positive and negative shear stresses are observed in the case of an inclined load for large vertical loads. However, for small vertical loads, the shear stresses become essentially negative in order to counter weight the horizontal external load. For the eccentric load, a non-symmetrical distribution with a gradually increasing separation distance with the eccentricity increase was observed but the total horizontal load was found close to zero, which is in agreement with the assumption of a vertical load.

References

Frydman, S. and Burd, J. H. (1997). "Numerical studies of bearing capacity factors N_γ." *J. of Geotech. & Geoenv. Engrg.*, ASCE, 123(1), 20-29.

Hjiaj, M., Lyamin, A.V. and Sloan, S.W. (2004). "Numerical limit analysis solutions for the bearing capacity factors N_γ." *Int. J. of solids and structures*, 42, 1681-1704.

Manoharan, N. and Dasgupta, S. P. (1995). "Bearing capacity of surface footings by finite elements." *Computers & Structures*, 54(4), 563-586.

Meyerhof, G.G. (1951). "The ultimate bearing capacity of foundations." *Géotechniqu*e, The Institution of Civil Engineers, London, 2, 301–332.

Soubra, A.-H. (1999). "Upper-bound solutions for bearing capacity of foundations." *J. of Geotech. & Geoenv. Engrg.,* ASCE*,* 125(1), 59-68.

Soubra, A.H., El-hachem, E., Oueidat, H. and Chehade, R. (2003a). "Bearing Capacity of Obliquely Loaded Footings." *CIMNA1, Beirut, Lebanon, 18p.*

Soubra, A.H., El-hachem, E., Oueidat, H. and Chehade, R. (2003b). "Bearing Capacity of Eccentricaly Loaded Footings." *CIMNA1*, Beirut, Lebanon, 18p.

Vesic, A. S. (1973). "Analysis of ultimate loads of shallow foundations." *Proc., ASC*E, 99(1), 45–73.

Yin, J.-H., Wang, Y.-J. and Selvadurai, P.S. (2001). "Influence of nonassociativity on the bearing capacity of a strip footing." *J. of Geotech. & Geoenv. Engrg.*, ASCE, 127(11), 985-989.

Zhu, M. and Michalowski, R. L. (2005). "Shape factors for limit loads on square rectangular footing." *J. of Geotech. & Geoenv. Engrg.*, ASCE, 131(2), 223-231.

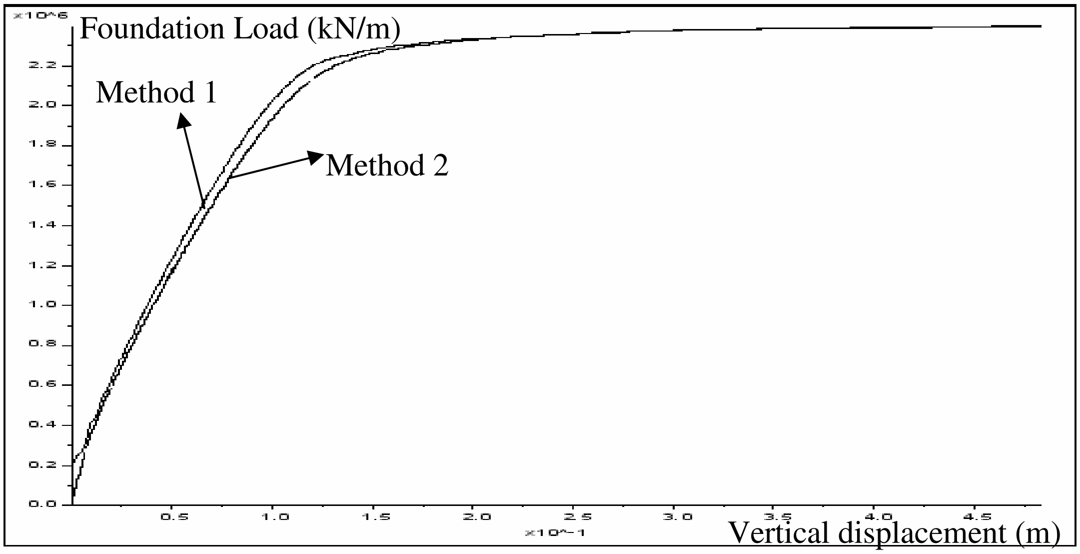

Figure 1: Foundation load – Displacement curves for the two methods

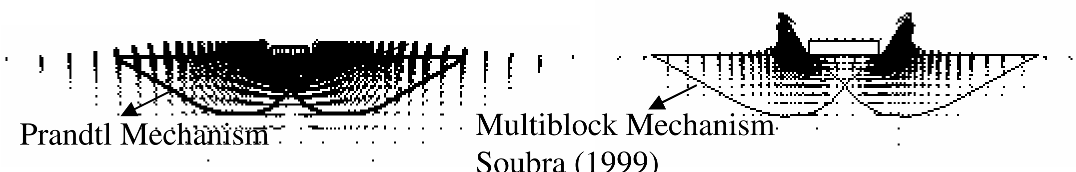

a) N_c **b)** N_γ

Figure 2: Failure mechanisms and $FLAC^{3D}$ velocity field

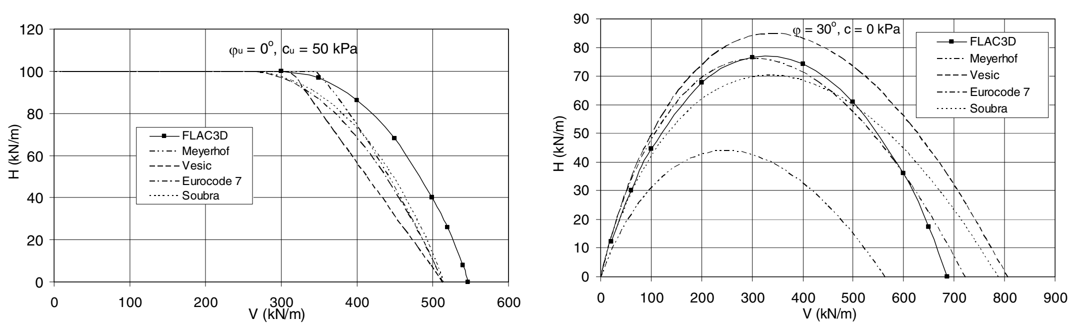

a) Clay **b) Sand**

Figure 3: Comparison of $(H-V)$ failure envelopes for a) clay and b) sand

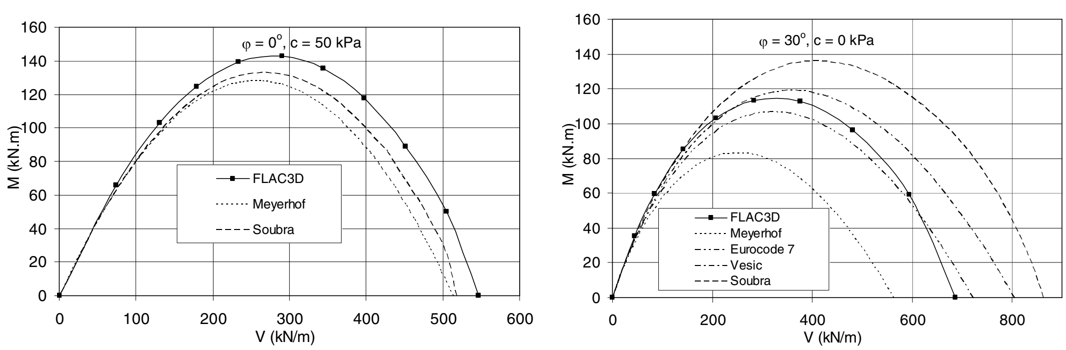

a) Clay **b) Sand**

Figure 4: Comparison of $(M-V)$ failure envelopes for a) clay and b) sand

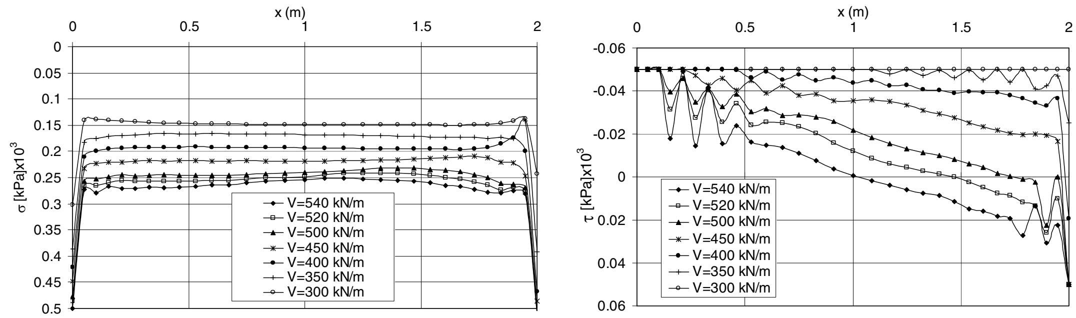

a) Clay

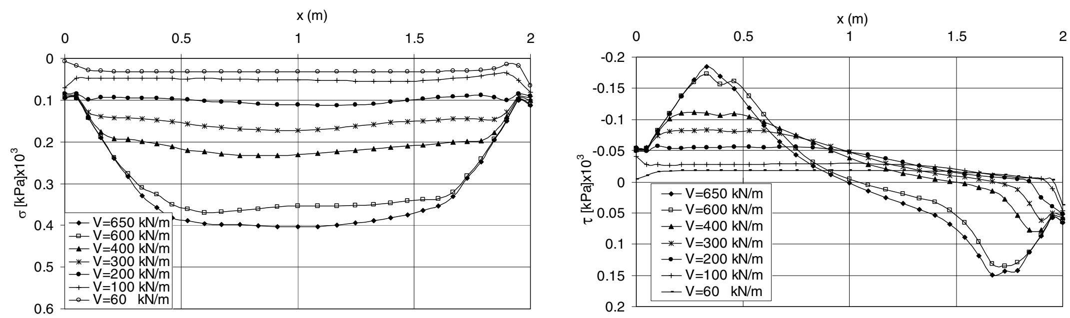

b) Sand

Figure 5: Normal $(\sigma)$and shear (τ) stress distributions at the base of the footing (x) in the case of inclined load for a) clay and b) sand

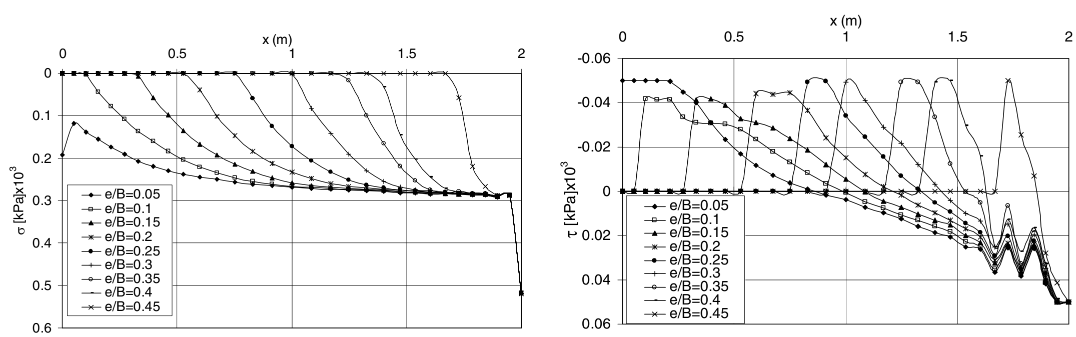

a) Clay

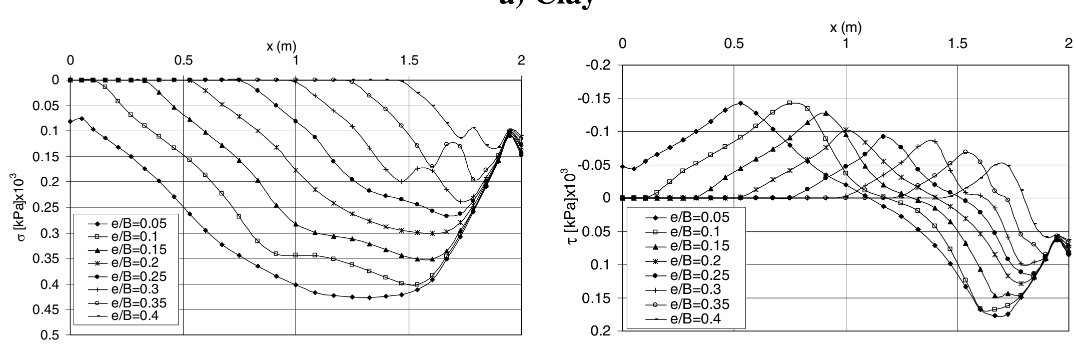

b) Sand

Figure 6: Normal (σ) and shear (τ) stress distributions at the base of the footing (x) in the case of eccentric load for a) clay and b) sand